Terahertz spectroscopic evidence of non-Fermi-liquid-like behavior in structurally modulated $PrNiO_3$ thin films

V. Eswara Phanindra, Piyush Agarwal, and D. S. Rana*
Indian Institute of Science Education and Research (IISER) Bhopal, M.P. 462066, INDIA

(Received 16 April 2017; published 11 January 2018)

The intertwined and competing energy scales of various interactions in rare-earth nickelates $RNiO_3$ (R = La to Lu) hold potential for a wide range of exotic ground states realized upon structural modulation. Using terahertz (THz) spectroscopy, the low-energy dynamics of a novel non-Fermi liquid (NFL) metallic phase induced in compressive $PrNiO_3$ thin film was studied by evaluating the quasiparticle scattering rate in the light of two distinct models over a wide temperature range. First, evaluating THz conductivity in the framework of extended Drude model, the frequency-dependent scattering rate is found to deviate from the Landau Fermi liquid (LFL) behavior, thus, suggesting NFL-like phase at THz frequencies. Second, fitting THz conductivity to the multiband Drude-Lorentz model reveals the band-dependent scattering rates and provides microscopic interpretation of the carriers contributing to the Drude modes. This is first evidence of NFL-like behavior in nickelates at THz frequencies consistent with dc conductivity, which also suggests that THz technology is indispensable in understanding emerging electronic phases and associated phenomena. We further demonstrate that the metal-insulator transition in nickelates has the potential to design efficient THz modulators.

DOI: 10.1103/PhysRevMaterials.2.015001

I. INTRODUCTION

Landau Fermi liquid (FL) theory well describes the metallic behavior in wide range of materials including heavy fermion systems, conventional metals, etc. [1]. According to this theory, the dc resistivity exhibits a temperature-dependent quadratic (i.e., $\rho \propto T^2$) behavior, which was attributed to the predominance of electron-electron interactions at low temperatures. The FL concept, however, breaks down for certain metals, which are tuned closer to the quantum phase transition (QPT) by nonthermal control parameters such as pressure, magnetic field, doping, etc. [1,2]. The study of such magnetic QPTs has gained considerable attention due to the observation of unusual ground states like non-Fermi-liquid (NFL) phases (e.g., $CeCu_{6-x}Au_x$ [3], $YbRh_2Si_2$ [4], MnSi [5], etc.) near/at the magnetic-to-nonmagnetic transition leading to a quantum critical point (QCP) [2,6]. Another important but different class of systems for such studies are RMO_3 (R, M = rare-earth, transition metal ion) perovskites. Of particular interest are strongly correlated transition-metal oxides with magnetically ordered ground states such as $RNiO_3$ nickelates [7], in which a metal-to-insulator transition (MIT) as well a magnetic to nonmagnetic transition can be tuned by variation of nonthermal control parameters (like external pressure, chemical composition, strain) resulting in a QPT at 0 K associated with quantum fluctuations [8–10]. The key aspect of these materials is that the interplay between spin, charge, and orbital degrees of freedom leads to the existence of several competing phases and in turn to complex and unusual phase diagrams [9,11].

The recent renewed interest in these nickelate systems was attributed to the possibility of controlling the MIT by heteroepitaxial strain, hydrostatic pressure, optical excitation, dimensionality, chemical doping, electric field [8,9,12], etc. As a result, the evolution of several novel electronic phases has made nickelates as potentially interesting candidates both from fundamental and applied point of view. Here, $PrNiO_3$ (PNO) and $NdNiO_3$ (NNO) are the only systems that exhibit simultaneous MIT and antiferromagnetic (AFM) order in the temperature range of 130–200 K. While $LaNiO_3$ lacks any MIT, magnetic order and remains metallic down to low temperatures, $SmNiO_3$ and other heavy rare-earth based systems exhibit disentangled MIT and magnetic order [7]. The extraordinary sensitivity of nickelates ground state to heteroepitaxial strain makes them ideal candidates for stabilization of various competing electronic and magnetic phases, which are absent in their bulk counterparts [9]. In $NdNiO_3$, for instance, the stabilization of NFL metallic state by Mikheev *et al.* [13], under compressive strain vis-a-vis an FL state under tensile strain points towards the underlying tunability of electronic phases upon subtle structural modulation in this compound. Such vulnerability of electronic phases is known to exist in other members too, hence, investigations by different techniques are needed. For example, our recent work on the metallic regime of PNO and NNO thin films [14,15] depicts that their dc transport behavior appears similar but the low-energy electronic phases as probed by terahertz spectroscopy are entirely different, as the former shows modified Drude-type conductivity [14] whereas the later exhibits a low-energy charge-density-wave excitation mode [15]. In PNO system, in particular, the THz-frequency-dependent optical conductivity and dielectric constant were observed to deviate from Drude-type behavior under different strain states. Such unusual electronic behavior requires extensive investigations to unveil fundamental properties of the concerned material.

The $PrNiO_3$ (PNO) system holds a very critical position in the phase diagram as (i) it lies next to metallic $LaNiO_3$ and

*dsrana@iiserb.ac.in

(ii) its MIT is most sensitive to the epitaxial strain, and, thus modified electronic phases require investigation by unconventional methodology. In this study, by means of terahertz (THz) spectroscopy supported by dc and Hall conductivities, we explore the novel features of strain modulated electronic phases in a $PrNiO_3$ thin film to potentially unravel the complexity of its ground state. THz time-domain spectroscopy (THz-TDS) in the frequency range of 0.2–1.5 THz was performed to study the quasiparticle response in the strain modified metallic state of PNO film. From extended Drude [16] model analysis, we show a clear deviation of the frequency-dependent scattering rate from FL theory assumptions suggesting NFL-like behavior at THz frequencies. We further propose that the MIT of the $RNiO_3$ films can be used to design THz transmission modulators.

II. EXPERIMENTAL DETAILS

A standard solid state reaction route was employed to prepare a dense polycrystalline bulk sample of $PrNiO_3$. This bulk target was used to deposit 60-nm-thick $PrNiO_3$ thin films on orthorhombic $NdGaO_3$ (NGO) (001) and $LaAlO_3$ (LAO) (100) oriented single-crystal substrates using pulsed laser deposition technique. Thus deposited PNO thin films on NGO(001) and LAO(100) substrates are referred as PNO/NGO, PNO/LAO films, respectively. A laser energy density of $2\,J/cm^2$, a pulse repetition rate of 4 Hz, a deposition temperature of 710 °C, oxygen pressure of 40 Pa during deposition, and 1000 Pa while cooling down to room temperature were optimized as deposition parameters. Structural measurements were performed on a PANalytical x-ray diffractometer equipped with a four-axis cradle. Reciprocal space maps (RSM's), φ, and rocking curves, θ-2θ scans, were performed to determine the coherent, epitaxial nature and phase purity of all the samples. The dc transport measurements of all the films were carried out in a four-point probe geometry in the temperature range of 2–300 K using a physical property measurement system (PPMS) [Quantum Design]. Hall measurements were performed in Van der Pauw geometry by tuning the magnetic field from −9 to 9 T over a temperature range of 2–300 K.

The terahertz-time domain spectroscopic (THz-TDS) measurements were performed in transmission mode employing a photoconductive antenna based THz-TDS spectrometer. Femtosecond laser pulses from a Ti:Al_2O_3 oscillator (100 fs, 800 nm, 82 MHz) excite the low-temperature grown GaAs (LT-GaAs) based photoconductive antennas, which acts as emitter and detector of THz radiation. Thus generated THz pulses were focused by silicon lens onto the sample placed in the closed cycle helium refrigerator (5–300 K) and the transmitted waveform from the sample is measured at the detector side. By using a variable optical delay line, the terahertz transient produced at the emitter side can be systematically delayed with respect to the gated detector, which allows us to scan the entire time-dependent THz wave form. By a subsequent Fourier transformation of the time-dependent terahertz wave form, the complex frequency spectrum is obtained, which then yields the transmission amplitude and phase shift, respectively. By solving the Fresnel's equations, we obtained the complex refractive index, which was used for the calculation of optical constants, namely optical conductivity, and dielectric permittivity spectra.

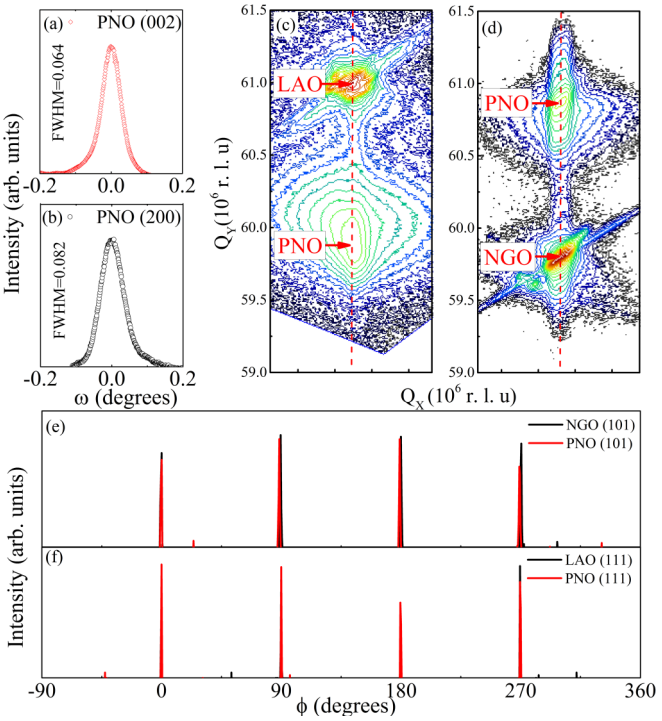

FIG. 1. [(a) and (b)] Rocking curves (ω scans) measured along (002) and (200) peaks of PNO films grown on NGO (001) and LAO (100) oriented substrates, respectively (FWHM values obtained from Gaussian fits to experimental data). [(c) and (d)] Reciprocal space maps obtained along (310) and (103) reflections of PNO films on LAO and NGO substrates, respectively. [(e) and (f)] φ scans acquired along (101) and (111) peaks for PNO/NGO and PNO/LAO films, respectively.

III. RESULTS AND DISCUSSION

A. Structural characterization

Figures 1(a) and 1(b) show the rocking curves (ω scans) acquired along (200), (002) peaks for PNO/LAO and PNO/NGO films (FWHM values corresponding to 0.082 and 0.064 obtained from Gaussian fits to the experimental data of PNO/LAO and PNO/NGO films, respectively). Similarly, the ω-2θ reciprocal space maps (RSM's) acquired along asymmetric (103) and (310) reflections as shown in Figs. 1(c) and 1(d) establish the coherently strained behavior of both films. This is evident from the fact that both the film and substrate peaks lie on the same pseudomorphic line. To establish the in-plane heteroepitaxial relationship of the film with respect to the substrate, φ scans were obtained along (111) and (101) peaks for PNO/LAO and PNO/NGO films, respectively. Four peaks in φ scans along with 90° separation evident from Figs. 1(e) and 1(f) for PNO/NGO and PNO/LAO films indicate a highly oriented nature and fourfold symmetry devoid of any twining effect. This confirms the in-plane epitaxial relationship of PNO films with respect to the underlying substrates. From these structural data it is also evident that PNO/LAO is compressively strained with lattice mismatch of −0.65%, whereas PNO/NGO is tensile strained with lattice strain of 1.33%.

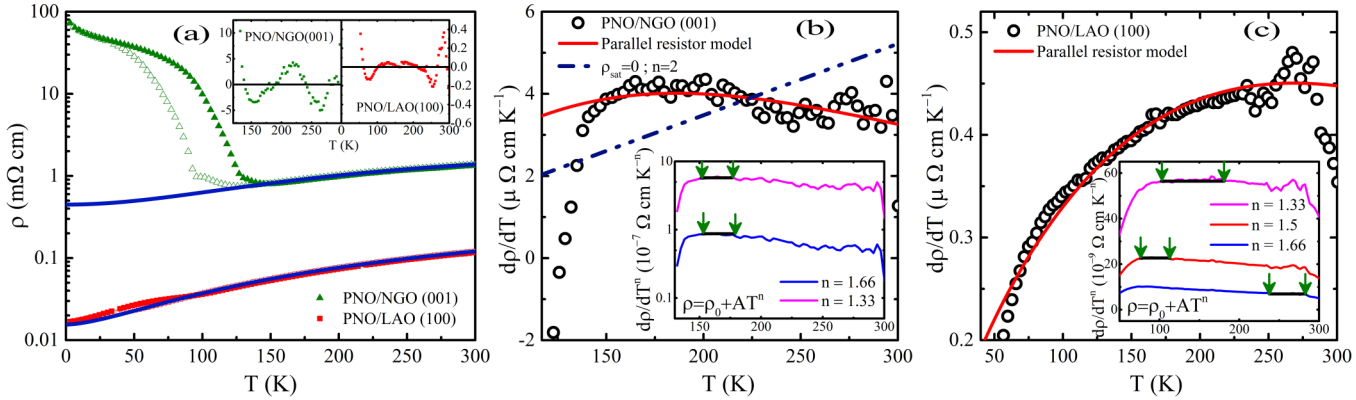

FIG. 2. (a) shows the temperature-dependent dc resistivity plots along with the parallel resistor model fits of coherently strained PNO films grown on LAO (100) and NGO (001) orientations, respectively. Regular residuals in the insets of (a) indicate the minimal fitting error. [(b) and (c)] Temperature-dependent resistivity derivatives analyzed in the context of parallel resistor model (red) and power-law equation (blue) for PNO films. Excluding the resistivity saturation (ρ_{sat}) term leads to the apparent changes in the power-law exponent (n) with respect to temperature, which can be visualized from the $\frac{d\rho}{dT^n}$ analysis [arrow symbols in the inset (b) and (c) indicate the limits within which data follow a power-law equation], thus signifying the superiority of the parallel resistor model analysis.

B. Direct-current transport data analysis

1. *Epitaxial strain driven tunable metal-insulator transition*

Figure 2(a) shows the temperature-dependent electrical resistivity of both PNO thin films [14]. It can be seen that the tensile strained PNO/NGO film shows insulating ground state with an insulator-metal transition temperature (T_{IM}) at 148 K. In contrast, the compressively strained PNO/LAO film exhibits a metallic behavior down to low temperatures with minor thermal hysteresis behavior at 90 K. Such kind of unusual behavior (i.e., quenching of insulating ground state due to external perturbations) in electrical resistivity was earlier observed in bulk PNO under large hydrostatic pressures [17,18]. The role of heteroepitaxial strain in the suppression of MIT in rare-earth nickelate films may be understood to arise from modifications in NiO_6 octahedra. The epitaxial strain, analogous to hydrostatic pressure, decreases the tilting of NiO_6 octahedra, consequently, altering the Ni-O-Ni bond angle. Straightening of this Ni-O-Ni bond angle lowers the MIT, thus, stabilizes the conducting ground state in the compressively strained PNO films as shown in Fig. 2 [14]. Overall, by hetero-epitaxial strain modulation, we successfully stabilized the conducting ground state under the influence of compressive strain, which can only be possible at very high pressures for a bulk PNO system.

2. *Epitaxial strain driven Fermi to non-Fermi liquid behavior*

From Fig. 2, we observed a clear transition from an antiferromagnetic-insulating phase (AFM-I) to a metallic ground state in PNO films under the influence of epitaxial strain [Fig. 2(a)]. To investigate whether this AFM-I (PNO/NGO) to metallic (PNO/LAO) phase crossover is accompanied by any novel electronic phase transition, we fitted our dc resistivity data with the parallel resistor model [Fig. 2(a)]. According to this model, in disordered materials, there exists a resistivity saturation channel which acts in parallel to usual Boltzmann electrical conduction, as a result, the total resistivity can be expressed as follows [13]:

$$\frac{1}{\rho(T)} = \frac{1}{\rho_0 + AT^n} + \frac{1}{\rho_{SAT}}. \quad (1)$$

Here, ρ_0 (residual resistivity), ρ_{sat} (saturation resistivity), and A (measure of electron-electron scattering strength) are fitting parameters (see Table I). From the dc resistivity analysis on PNO/NGO and PNO/LAO films, we found an intriguing FL to NFL crossover behavior. As evident from Table I, the temperature exponent "n" varies from 2.01(6/3) to 1.62(5/3) for tensile and compressive films, respectively. The power-law exponent $n = 2$, 1.62 corresponds to the FL and NFL behaviors, respectively. Figures 2(b) and 2(c) show the temperature-dependent resistivity derivatives analyzed in the context of parallel resistor model, which successfully describe dc resistivity data and yield exponents $n \approx 5/3$ and ≈ 2 for PNO/LAO and PNO/NGO films, respectively. In contrast, resistivity analysis by a power-law model [i.e., excluding the saturation resistivity ($\rho_{sat} = 0$) term] leads to apparent changes in the power-law exponent with respect to temperature [the

TABLE I. MIT temperatures, lattice mismatches of PNO films, and dc resistivity fit parameters to the parallel resistor model (as shown in Fig. 2). Here, A, n, ρ_{sat}, ρ_0 are the best fit parameters.

Sample	T_{IM}(K)	A × 10^{-8} (Ω cm)	n	ρ_{sat} (mΩ cm)	ρ_0 × 10^{-3} (Ω cm)	Lattice mismatch (%)
PNO/NGO(001)	148	3.03	2.01	2.38	0.55	1.33
PNO/LAO(100)	0	1.37	1.62	0.49	0.016	−0.65

limits within which the experimental data follow a power-law equation are indicated by arrow symbols in the insets of Figs. 2(b) and 2(c)] thereby unable to explain the dc resistivity data, which eventually resorted us to employ the parallel resistor model to describe the dc resistivity behavior of PNO thin films. Also, robust $\rho \propto T^2$ behaviors in resistivity along with little or no phonon scattering (which yields $\rho \propto T^5$ behavior below the Debye Temperature ≈420 K for the case of nickelates [9]) were often found in many perovskites notably in cuprate superconductors, which exhibit T^2 behavior extending to room temperature in some parts of their phase diagrams [19,20], in rare-earth nickelates [13] and in titanates [21] as well.

Additionally, when there are multiple conduction bands, as is the case for nickelates [22,23] and titanates [21,24], electron-electron scattering can proceed through both intra and interband transitions [21]. In case of an interband scattering event, the total current can change via electron transfer between bands (with dissimilar effective masses), leading to resistance from electron-electron scattering (in addition to umklapp process [25]). Besides, short-range Coulomb interactions are also strong for conduction bands resulting from the localized $3d$ orbitals (as in the case of Ni, Ti, etc.), which leads to an enhancement/dominance of electron-electron scattering eventually screening out the optical phonon mode scattering (which operates at high temperatures) [21]. Overall, based on the quadratic temperature dependence of ρ(T) and the non-Drude feature evident from the THz conductivity spectra [14], we inferred that electron-electron correlations play a significant role in the electrical transport of PNO/NGO thus consistent with the previous reports [26].

From Fig. 2(a), as one traverses from tensile (PNO/NGO) to compressive (PNO/LAO) strain regime ($\varepsilon_{xx} = 1.33\% \rightarrow \varepsilon_{xx} = -0.65\%$), the temperature-driven MIT is completely quenched and an unusual metallic ground-state emerges, which exhibits an NFL behavior [8–10,13]. This NFL phase appears to be caused by spin fluctuations when the transition temperature $T_{IM} = T_N$ is suppressed down to zero Kelvin under the effect of compressive strain. Such electronic phase crossovers (FL to NFL behavior) were observed earlier under the effect of large external hydrostatic pressures ≈50 kbar in PNO bulk polycrystalline samples [8]. Hence we emphasize that heteroepitaxial strain (ε_x) is highly efficient and an alternative route to external perturbations like hydrostatic pressure P_c, doping x_c, and magnetic field H_c, which modulate/stabilize the novel electronic phases.

C. Temperature-dependent Hall coefficient and carrier mobility

The Hall resistivity measurements and temperature-dependent Hall coefficient can effectively track the changes in the electronic structure across the MIT in $RNiO_3$ nickelates. In this regard, here we have performed the Hall resistivity measurements in the newly stabilized metallic ground state (in an otherwise AFM insulator) of PNO/LAO down to low temperatures as shown in the Fig. 3. To obtain the Hall coefficient ($R_H = \partial\rho_{xy}/\partial B$), we firstly acquired Hall resistivity by eliminating the magnetoresistivity contribution as

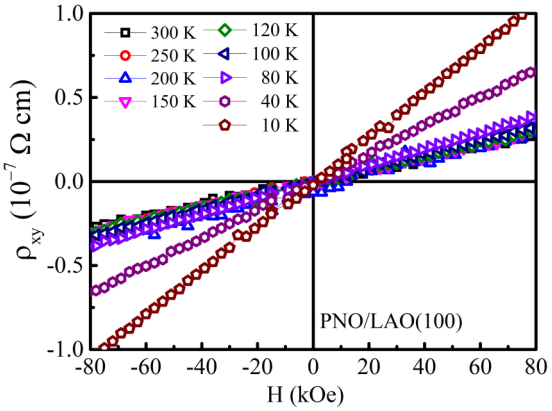

FIG. 3. Magnetic field dependent Hall resistivity (ρ_{xy}) plots of PNO/LAO film measured at various temperatures. The slope R_H (i.e., ρ_{xy} vs H) remains positive down to low temperatures indicating holes as majority charge carriers.

follows:

$$\rho_{xy} = [V_H(B) - V_H(-B)]\,\frac{t}{2I},$$

where t is the film thickness, $V_H(\pm B)$ are the Hall voltages measured at positive and negative magnetic fields, respectively, and I is the current applied perpendicular to the magnetic field direction. Analysis of the temperature-dependent Hall coefficient of PNO/LAO film suggests the majority charge carriers are holelike, which is consistent with previous reports [23,27]. By substituting the Hall coefficient and dc resistivity values in the relation $\mu = \frac{R_H}{\rho}$, we obtained carrier mobility values as $0.27\,\mathrm{cm^2\,V^{-1}\,s^{-1}}$ at 300 K and $7.5\,\mathrm{cm^2\,V^{-1}\,s^{-1}}$ at 10 K [14]. The Hall coefficient R_H remains positive and increases monotonically with decreasing temperature without any sign crossover. In previous studies on nickelates, particularly on bulk $PrNiO_3$ and $SmNiO_3$ thin films, an R_H sign crossover from positive to negative was observed near T_N, which depicts reversal of majority charge carriers from hole to electronlike. Such kind of sign reversal or charge compensation behavior was attributed to the electronic structure modification by the onset of AFM ordering coupled with the formation of a spin density wave (SDW) [23]. Alternatively, such R_H sign crossovers were attributed to opening of gap at the Fermi surface, thereby, leading to charge compensation in $NdNiO_3$ films [28]. In the present case, absence of any such R_H sign crossover suggests that holes are the majority carriers down to low temperatures. It also suggests absence of AFM ordering/formation of SDW in PNO/LAO films over a wide temperature range as shown in Fig. 3.

D. Terahertz spectroscopic data on PNO/LAO film

Here we discuss the characteristic features of complex conductivity spectra of a PNO/LAO film as shown in Figs. 4(a) and 4(b). As the temperature increases, the Drude peak evident at lower frequencies decreases and becomes less prominent as shown in Fig. 4(a). Furthermore, the real part of THz conductivity (σ_1) versus T plot of PNO/LAO film shows metallic behavior down to low temperatures, sans any electronic first-order phase transition typically seen for rare-earth

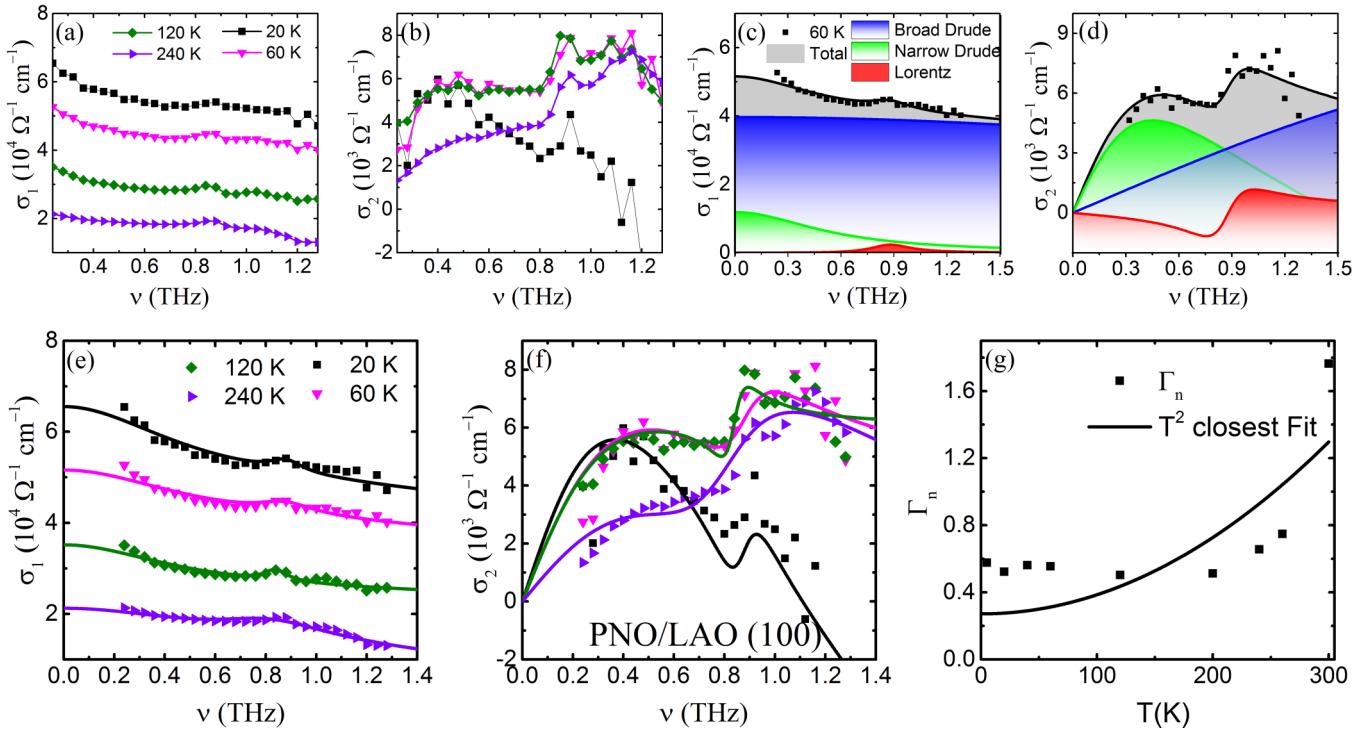

FIG. 4. [(a) and (b)] Complex conductivity spectra of the PNO/LAO thin film at various temperatures. Similarly, (e), (f), (c), and (d) show the simultaneous fits (solid lines) of real and imaginary parts of the complex conductivity spectra (symbols) to the Drude-Lorentz model at selected temperatures and their decomposition into individual Drude and Lorentz terms. (g) T-dependent quasiparticle scattering rate (Γ_n) obtained from the narrow Drude component. Here, the solid line depicts the best FL-like fit, which is unable to reproduce the experimental data indicating deviation from FL behavior.

nickelates. In the subsequent sections, we analyze the THz conductivity spectra in the context of the two most relevant models which discuss both the frequency-independent and frequency-dependent scattering rate behaviors and provide significant insights into the physics of PNO systems.

1. Decomposition of THz-range optical conductivity: Drude-Lorentz model with two Drude modes (PNO/LAO film)

In the subsequent steps, we used a Drude-Lorentz (D-L) model with one Lorentz term and two Drude terms (D_1 is a narrow Drude component and D_2 is a comparatively broad component) to account for the THz electronic response arising from multiple electronic subsystems with distinct properties [29]. In this regard, the Drude modes account for the free-carrier contribution, and a Lorentz (L) contribution arises from the minor insulating region (evident as minor thermal hysteresis in dc resistivity data of PNO/LAO film). Such analysis is in part motivated by the multiband nature of nickelates and by the observation of two distinct types of carriers participating in the charge transport [23]. While there are multiple bands (i.e., an electronlike Fermi pocket at the Brillouin zone center and holelike Fermi pockets at the zone corners) crossing the Fermi level as predicted in analogue $NdNiO_3/LaAlO_3$ films from band-structure calculations and an ARPES study [22], for the sake of convergence of fits as well as to reduce the number of fitting parameters, we have adopted a minimal description that considers only two sets of carriers by gathering multiple carrier bands into single electron and hole pockets using the two-component D-L model. Similar analysis was previously adopted in iron pnictide superconductors, topological insulators, Sr_2RuO_4 systems, etc. [30–32]. Hence according to the D-L model, the complex conductivity can be modeled as follows [31]:

$$\tilde{\sigma}(\omega) = \frac{1}{4\pi}\left[\sum_j \frac{\omega_{j,p}^2}{\gamma_j - i\omega} + \sum_n \frac{\omega_{n,pL}^2 \omega}{i\left(\omega_{n,L}^2 - \omega^2\right) + \omega\gamma_{n,L}} - i\omega(\epsilon_\infty - 1)\right], \quad (2)$$

where the fitting parameters $\omega_{j,p}$, γ_j, and ε_∞ denote the Drude plasma frequency, the scattering rate of Drude carriers, and the dielectric constant at high frequencies, respectively. $\omega_{n,L}$, $\omega_{n,pL}$, and $\gamma_{n,L}$ are the center peak frequency, the plasma frequency, and the scattering rate of the nth Lorentz component, respectively. Thus measured real and imaginary parts (σ_1 and σ_2) of the THz conductivity spectra of PNO/LAO thin film at each temperature are simultaneously fitted with the D-L model and the corresponding fitting parameters are tabulated in Table II. Figures 4(c)–4(g) summarizes the simultaneous fits and their decomposition into individual Drude and Lorentz contributions at $T = 60$ K. From Table II, we discern that the broad Drude (D_2) term acquires the majority of the free carriers and displays a large scattering rate in comparison to the narrow Drude mode (D_1). This is consistent with previously reported optical studies [29]. Figure 4(g) shows the T dependence of the narrow Drude scattering rate (Γ_n), which is roughly

TABLE II. Temperature-dependent fitting parameters of complex conductivity spectra (Fig. 4) to the D-L model and its decomposition into individual Drude and Lorentz contributions along with the calculated total dc conductivity and resistivity data of the PNO/LAO thin film.

	PNO/LAO (100)	20 K	60 K	120 K	240 K
Lorentz	$\omega_0/2\pi$(THz)	0.88	0.88	0.84	0.84
	γ_L(THz)	0.16	0.27	0.11	0.54
	$\omega_{pL}/2\pi$(THz)	70.62	89.37	58.27	156.71
Narrow Drude	$\omega_p/2\pi$(THz)	339	288	254	234
	Γ_d(THz)	0.52	0.56	0.50	0.66
Broad Drude	$\omega_p/2\pi$(THz)	1845	1755	1546	624
	Γ_d(THz)	5.63	6.17	7.62	2.12
Total	$\sigma_0(10^4\,\Omega^{-1}\,\mathrm{cm}^{-1})$	6.55	5.16	3.52	2.13
	$\rho(10^{-5}\,\Omega\,\mathrm{cm})$	1.52	1.94	2.84	4.71

constant in the temperature range of 5–200 K and increases anomalously with increasing temperature, which cannot be interpreted in terms of conventional FL behavior. In addition, the plasma frequencies of both the narrow and broad Drude components gradually decreases with respect to temperature (Table II) suggesting the loss of itinerant charge carriers (i.e., transfer of spectral weight) from lower energies to higher binding energies. This is reminiscent of bad metallic behavior usually observed in rare-earth nickelates [33]. Overall, the D-L model with two Drude modes successfully describes the THz conductivity data, with one Drude component (D_2) accounting for most of the spectral weight, thereby being much broader than the other component (D_1). Also, such decomposition not only fits the experimental data well but it also gives the microscopic interpretation (i.e., electrons-D_1 and holes-D_2) of the charge carriers contributing to the Drude modes and their temperature-dependent behavior.

2. *Extended Drude analysis-implications of NFL-like behavior in PNO/LAO film*

On strict terms, the NFL behavior cannot be extracted self-sufficiently from dc resistivity curves measured at high temperatures due to the influence of electron-phonon scattering process. In correlated oxides, parallel resistor model with additional saturation resistivity term has been frequently employed to deduce the temperature exponents. However, in order to substantiate the NFL behavior deduced from the dc resistivity analysis, we have analyzed the THz conductivity spectra using an extended Drude formalism. Here, we invoke the extended Drude phenomenology, which has been extensively applied to examine the applicability of Landau Fermi liquid (LFL) theory and to describe the optical conductivity spectra in heavy fermion systems [35] and transition metal oxides [34] including rare-earth nickelates [33].

Unlike D-L model, it considers a frequency-dependent scattering rate, thereby, replacing the frequency-independent scattering rate. According to Boltzmann transport theory, the frequency-dependent scattering rate is considered as a natural analog to temperature-dependent dc resistivity thus allows us to probe the deviations from the FL (i.e., ω^2 dependence) behavior. According to the extended Drude model, the scattering

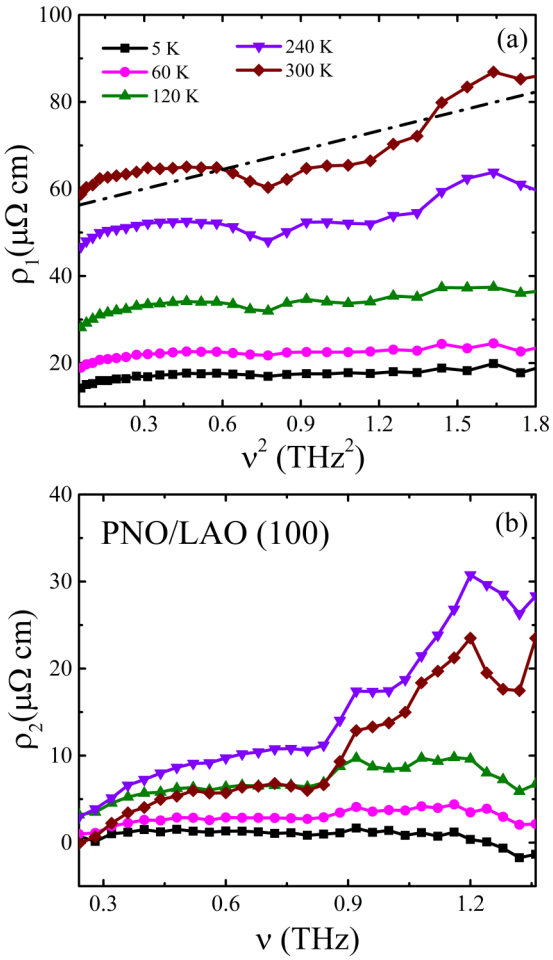

FIG. 5. (a) shows the real part $\rho_1(\omega)$ for the PNO/LAO (100) thin film. Here the dashed line depicts the deviation from linearity in ω^2 domain. Similarly, (b) shows the imaginary part $\rho_2(\omega)$ as a function of frequency. Both plots represent the nonlinear behavior (as described in the text) in ω^2 and ω domain implying an NFL-like behavior.

rate $\Gamma(\omega)$ can be related to the σ_1 and σ_2 as follows [34]:

$$\rho_1(\omega) = \frac{\Gamma(\omega)}{\epsilon_0\omega_p^2} = \frac{\sigma_1(\omega)}{\sigma_1(\omega)^2 + \sigma_2(\omega)^2}.$$

Here, $\omega_p^2 = \sum_i \frac{N_i e^2}{m_i^* \epsilon_0}$ is the plasma frequency and $\rho_1(\omega)$ is the real part of the frequency-dependent resistivity $[\tilde{\rho}(\omega) = \rho_1(\omega) + i\,\rho_2(\omega) = 1/\tilde{\sigma}(\omega)]$. The real $[\rho_1(\omega)]$ and imaginary $[\rho_2(\omega) = \frac{\sigma_2(\omega)}{\sigma_1(\omega)^2+\sigma_2(\omega)^2}]$ parts can be used as measures of the scattering strength $[\Gamma(\omega)]$ and effective mass $[m*(\omega)]$ of charge carriers, respectively. Figure 5(a) shows the $\rho_1(\omega)$ in the temperature range of 5–120 K. Here, $\rho_1(\omega)$ clearly deviates from the ω^2 behavior, and hence is incompatible with the quadratic FL behavior, which predicts the frequency and temperature-dependent scattering rate to differ by a factor of 4π [2] via the relation $\Gamma(\omega) = A[(\hbar\omega)^2 + (2\pi k_B T)^2]$ [35]. Now we turn to the imaginary part $\rho_2(\omega)$ of the PNO/LAO film as shown in Fig. 5(b). For systems obeying the Landau's FL theory, the imaginary part $\rho_2(\omega)$ should display a frequency-dependent linear behavior [36,37], which is in quite contrary to the observed result [Fig. 5(b)]. This suggests an NFL-like behavior at THz frequencies in PNO/LAO thin films.

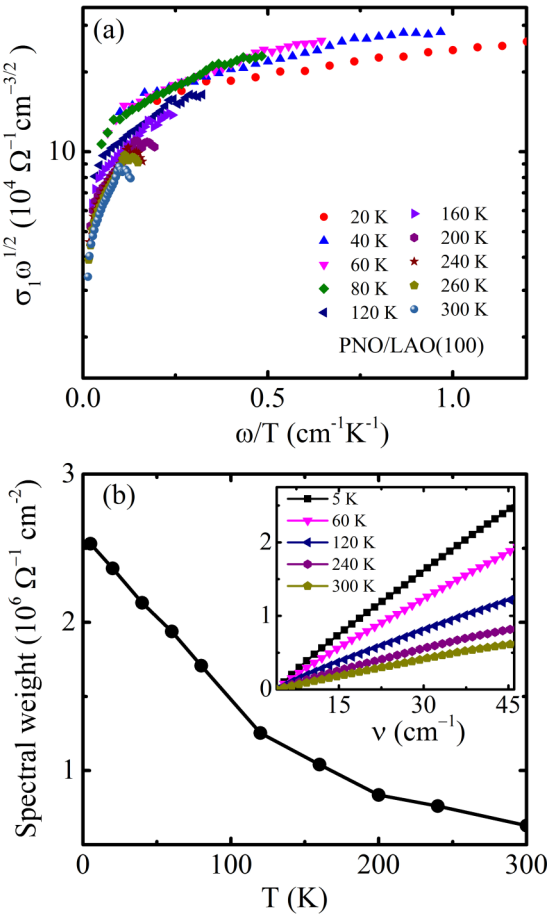

FIG. 6. (a) shows the frequency-/temperature-dependent scaling behavior of $\sigma_1(\omega)$ of PNO/LAO thin film. Here solid symbols denote the $\sigma_1\omega^{1/2}$ plotted as a function of ω/T. (b) shows the temperature-dependent spectral weight (S.W.) behavior of the PNO/LAO film, and the inset of (b) depicts the partial sums of frequency-dependent S.W. calculated at various temperatures.

In order to examine any quantum critical features associated with thus stabilized NFL-like phase in PNO/LAO thin films, we have performed a scaling analysis. Scaling plots were initially proposed and discussed as signatures of quantum critical behavior, although later denied [38]. To present our data in the context of scaling phenomenology, we plotted our THz conductivity data of the PNO/LAO film as per the equation

$$\sigma_1(\omega,T) \sim \omega^{-1/2}Z(\omega/T). \quad (3)$$

From Fig. 6(a), it can be seen that all $\sigma_1(\omega)$ curves obey the scaling function $Z(\omega/T)$ and thereby converge into a unique scaling relationship as given by Eq. (3) [34,39]. The observed collapse of THz conductivity data (measured at various temperatures) into a single scaling plot [Fig. 6(a)] may be an indication of quantum critical behavior in the PNO/LAO thin film [34,39], thus consistent with the previous reports on ruthenates and high-T_c superconductors [40].

According to Zhou *et al.* [8], the physical properties associated with an order-disorder transition, although it is a first order, may acquire some quantum critical characteristic features when the transition temperature is reduced to near zero Kelvin, by nonthermal external perturbations such as magnetic field, hydrostatic pressure, etc. [8] As a result, new ground states such as NFL behavior due to critical spin fluctuations commonly occur on the disorder side of the transition in the vicinity of a quantum critical point (QCP) [41,42]. Hence we interpret that the existence of instabilities of an itinerant Fermi surface or spin fluctuations plausible for these systems [22,43] may be the underlying phenomena that give rise to the observed NFL-like behavior in the PNO thin film.

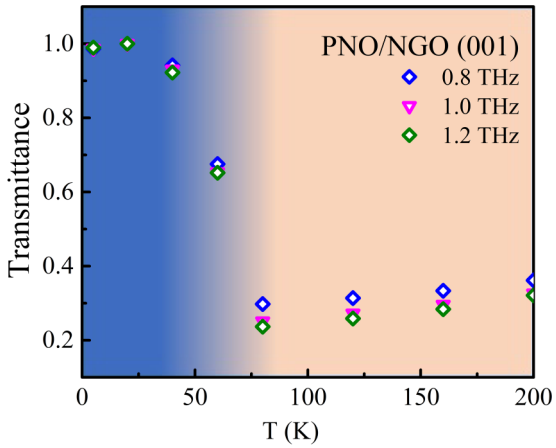

FIG. 7. Temperature-dependent terahertz transmittance of PNO/NGO (001) thin film. For comparison, the transmittance data are normalized with the transmittance at 20 K. Here, blue (brown) color regions indicate the insulating (metallic) regimes, respectively.

3. Bad metallic behavior as evident from the spectral weight data analysis

In addition to above-mentioned phenomena, any kind of soft gaps and pseudogaps may have strong influence on the transport properties and spectral weight behavior near and above the I-M transition [44,45]. In view of this, we extracted the spectral weight (S.W) [S.W. $= \int \sigma_1(\omega)d\omega$] from the THz-range optical conductivity spectra and analyzed its temperature-dependent behavior for a PNO/LAO thin film as shown in Fig. 6(b). This figure depicts a monotonous decrease of S.W. for a compressively strained PNO/LAO film in the metallic regime. This phenomenon is in contrast to the conventional metals since good metals are expected to show constant spectral weight with respect to temperature. The observed decrease of spectral weight in the PNO film signifies a bad metallic behavior, which occurs due to transfer of charge carriers from coherent to incoherent states [33].

In addition to the above mentioned fundamental facets revealing the NFL-like behavior at THz frequencies, an applied aspect associated with MIT was also evaluated. We show that the RNiO$_3$ (R = rare earth) thin films can be employed as temperature-tuned analog THz modulators [46] since the MIT in RNiO$_3$ nickelates can be tuned to room temperature by altering epitaxial strain, rare-earth cation size, etc. [47,48]. Figure 7 shows the normalized transmittance (normalized with the transmittance measured at 20 K) of a PNO/NGO (001)-60 nm film plotted as a function of temperature. It can be seen that the transmittance changes by about 50% as one traversed across MIT. This suggests that nickelates are potential candidates for

the design of efficient temperature-driven THz transmittance modulators.

IV. SUMMARY AND OUTLOOK

Using THz spectroscopy, we have unveiled some novel attributes of the complex ground state of epitaxial engineered metallic PNO thin films by studying the quasiparticle scattering rate behavior in the light of two distinct models over a wide temperature range. By performing the extended Drude model analysis and multiband Drude-Lorentz analysis of the THz conductivity spectra, we provide the first experimental evidence of NFL-like behavior in structurally modulated PNO thin films at THz frequencies. This study further emphasizes the indispensable role of THz spectroscopy in unraveling the heteroepitaxy stabilized NFL-like phase and associated phenomena in nickelate thin films. These studies prompt us to propose the implementation of temperature-dependent THz spectroscopy along with the variation of magnetic field and time-resolved aspects to potentially unravel the hidden phases (having an origin in magnetic order) in nickelates, in particular, and complex magnetic oxides, in general.

ACKNOWLEDGMENTS

D.S.R. thanks the Science and Engineering Research Board (SERB), Department of Science and Technology, New Delhi, for financial support under research Project No. EMR/2016/003598. Financial support of DST-FIST program [Project No. SR/FST/PSl-195/2014(C)] is thankfully acknowledged.

[1] A. Schofield, P. B. Rock, and M. A. Georgeson, Vision Res. **51**, (1998).
[2] G. R. Stewart, Rev. Mod. Phys. **73**, 797 (2001).
[3] H. Löhneysen, S. Mock, A. Neubert, T. Pietrus, A. Rosch, A. Schröder, O. Stockert, and U. Tutsch, J. Magn. Magn. Mater. **177**, 12 (1998).
[4] O. Trovarelli, C. Geibel, S. Mederle, C. Langhammer, F. M. Grosche, P. Gegenwart, M. Lang, G. Sparn, and F. Steglich, Phys. Rev. Lett. **85**, 626 (2000).
[5] E. Kim and M. H. W. Chan, Nature (London) **427**, 225 (2004).
[6] Buttgen, A. Gunther, S. Widmann, S. Riegg, A. Krimmel, and A. Loidl, J. Low Temp. Phys. **161**, 148 (2010).
[7] M. L. Medarde, J. Phys. Condens. Matter **9**, 1679 (1997).
[8] J.-S. Zhou, J. B. Goodenough, and B. Dabrowski, Phys. Rev. Lett. **94**, 226602 (2005).
[9] J. Liu, M. Kargarian, M. Kareev, B. Gray, P. J. Ryan, A. Cruz, N. Tahir, Y.-D. Chuang, J. Guo, J. M. Rondinelli, J. W. Freeland, G. A. Fiete, and J. Chakhalian, Nat. Commun. **4**, 2714 (2013).
[10] H. Kobayashi, S. Ikeda, Y. Yoda, N. Hirao, Y. Ohishi, J. A. Alonso, M. J. Martinez-Lope, R. Lengsdorf, D. I. Khomskii, and M. M. Abd-Elmeguid, Phys. Rev. B **91**, 195148 (2015).
[11] B. A. Frandsen, L. Liu, S. C. Cheung, Z. Guguchia, R. Khasanov, E. Morenzoni, T. J. S. Munsie, A. M. Hallas, M. N. Wilson, Y. Cai, G.M. Luke, B. Chen, W. Li, C. Jin, C. Ding, S. Guo, F. Ning, T. U. Ito, W. Higemoto, S. J. L. Billinge, S. Sakamoto, A. Fujimori, T. Murakami, H. Kageyama, J. A. Alonso, G. Kotliar, M. Imada, and Y. J. Uemura, Nat. Commun. **7**, 12519 (2016).
[12] W. Hu, S. Catalano, M. Gibert, J.-M. Triscone, and A. Cavalleri, Phys. Rev. B **93**, 161107 (2016).
[13] E. Mikheev, A.J. Hauser, B. Himmetoglu, N. E. Moreno, A. Janotti, C. G. Van de Walle, and S. Stemmer, Sci. Adv. **1**, e1500797 (2015).
[14] V. E. Phanindra, S. Das, K. S. Kumar, P. Agarwal, R. Rana, and D. S. Rana, Phys. Rev. B **95**, 085114 (2017).
[15] R. Rana, P. Pandey, S. S. Prabhu, and D. S. Rana, arXiv:1412.3244.
[16] S. V. Dordevic and D. N. Basov, Ann. Phys. **15**, 545 (2006).
[17] P. C. Canfield, J. D. Thompson, S. W. Cheong, and L. W. Rupp, Phys. Rev. B **47**, 12357 (1993).
[18] X. Obradors, L. M. Paulius, M. B. Maple, J.B. Torrance, A.I. Nazzal, J. Fontcuberta, and X. Granados, Phys. Rev. B **47**, 12353 (1993).
[19] N. Barisic, M. K. Chan, Y. Li, G. Yu, X. Zhao, M. Dressel, A. Smontara, and M. Greven, Proc. Natl. Acad. Sci. USA **110**, 12235 (2013).
[20] R. A. Cooper, Y. Wang, B. Vignolle, O. J. Lipscombe, S. M. Hayden, Y. Tanabe, T. Adachi, Y. Koike, M. Nohara, H. Takagi, C. Proust, and N. E. Hussey, Science **323**, 603 (2009).
[21] E. Mikheev, B. Himmetoglu, A. P. Kajdos, P. Moetakef, T. A. Cain, C. G. Van de Walle, and S. Stemmer, Appl. Phys. Lett. **106**, 062102 (2015).
[22] R. S. Dhaka, T. Das, N. C. Plumb, Z. Ristic, W. Kong, C. E. Matt, N. Xu, K. Dolui, E. Razzoli, M. Medarde, L. Patthey, M. Shi, M. Radović, and J. Mesot, Phys. Rev. B **92**, 035127 (2015).
[23] S. D. Ha, R. Jaramillo, D. M. Silevitch, F. Schoofs, K. Kerman, J. D. Baniecki, and S. Ramanathan, Phys. Rev. B **87**, 125150 (2013).
[24] P. Moetakef, C. A. Jackson, J. Hwang, L. Balents, S. J. Allen, and S. Stemmer, Phys. Rev. B **86**, 201102 (2012).
[25] J. Appel, Phys. Rev. **125**, 1815 (1962).
[26] D. Oka, Y. Hirose, S. Nakao, T. Fukumura, and T. Hasegawa, Phys. Rev. B **92**, 205102 (2015).
[27] S.-W. Cheong, H. Y. Hwang, B. Batlogg, A. S. Cooper, and P. C. Canfield, Phys. B Condens. Matter **194**, 1087 (1994).
[28] A. J. Hauser, E. Mikheev, N. E. Moreno, T. A. Cain, J. Hwang, J. Y. Zhang, and S. Stemmer, Appl. Phys. Lett. **103**, 182105 (2013).
[29] Y. M. Dai, B. Xu, B. Shen, H. Xiao, H. H. Wen, X. G. Qiu, C. C. Homes, and R. P. S. M. Lobo, Phys. Rev. Lett. **111**, 117001 (2013).
[30] N. Barišić, D. Wu, M. Dressel, L. J. Li, G. H. Cao, and Z. A. Xu, Phys. Rev. B **82**, 054518 (2010).
[31] C. S. Tang, B. Xia, X. Zou, S. Chen, H.-W. Ou, L. Wang, A. Rusydi, J.-X. Zhu, and E. E. M. Chia, Sci. Rep. **3**, 3513 (2013).
[32] Y. Takahashi, S. Chakraverty, M. Kawasaki, H. Y. Hwang, and Y. Tokura, Phys. Rev. B **89**, 165116 (2014).
[33] R. Jaramillo, S. D. Ha, D. M. Silevitch, and S. Ramanathan, Nat. Phys. **10**, 304 (2014).
[34] D. Geiger, U. S. Pracht, M. Dressel, J. Mravlje, M. Schneider, P. Gegenwart, and M. Scheffler, Phys. Rev. B **93**, 165131 (2016).

[35] G. Bossé, L. D. Pan, Y. S. Li, L. H. Greene, J. Eckstein, and N. P. Armitage, Phys. Rev. B **93**, 085104 (2016).
[36] D. Stricker, J. Mravlje, C. Berthod, R. Fittipaldi, A. Vecchione, A. Georges, and D. van der Marel, Phys. Rev. Lett. **113**, 087404 (2014).
[37] C. Berthod, J. Mravlje, X. Deng, R. Žitko, D. van der Marel, and A. Georges, Phys. Rev. B **87**, 115109 (2013).
[38] S. Kamal, D. M. Kim, C. B. Eom, and J. S. Dodge, Phys. Rev. B **74**, 165115 (2006).
[39] Y. S. Lee, J. Yu, J. S. Lee, T. W. Noh, T.-H. Gimm, H.-Y. Choi, and C.B. Eom, Phys. Rev. B **66**, 041104 (2002).
[40] S. Kamal, J. Dodge, D.-M. Kim, and C. B. Eom, in *Quantum Electronics and Laser Science Conference, 2005, QELS'05* (IEEE, Baltimore, 2005), pp. 443–445.
[41] K. H. Kim, N. Harrison, M. Jaime, G. S. Boebinger, and J. A. Mydosh, Phys. Rev. Lett. **91**, 256401 (2003).
[42] J. Custers, P. Gegenwart, H. Wilhelm, K. Neumaier, Y. Tokiwa, O. Trovarelli, C. Geibel, F. Steglich, C. Pépin, and P. Coleman, Nature **424**, 524 (2003).
[43] S. J. Allen, A. J. Hauser, E. Mikheev, J. Y. Zhang, N. E. Moreno, J. Son, D. G. Ouellette, J. Kally, A. Kozhanov, L. Balents, and S. Stemmer, APL Mater. **3**, 062503 (2015).
[44] D. D. Sarma, N. Shanthi, and P. Mahadevan, J. Phys. Condens. Matter **6**, 10467 (1994).
[45] M. K. Stewart, J. Liu, M. Kareev, J. Chakhalian, and D. N. Basov, Phys. Rev. Lett. **107**, 176401 (2011).
[46] G. Karaoglan-Bebek, M. N. F. Hoque, M. Holtz, Z. Fan, and A. A. Bernussi, Appl. Phys. Lett. **105**, 201902 (2014).
[47] G. Catalan, Phase Transit. **81**, 729 (2008).
[48] S. Catalano, M. Gibert, V. Bisogni, F. He, R. Sutarto, M. Viret, P. Zubko, R. Scherwitzl, G. A. Sawatzky, T. Schmitt, and J.-M. Triscone, APL Mater. **3**, 062506 (2015).